



Contrasting physical properties of black carbon in urban Beijing between winter and summer

5 Dantong Liu^{1,2}, Rutambhara Joshi^{2,5}, Junfeng Wang⁴, Chenjie Yu², James D. Allan^{2,5},
Hugh Coe², Michael J. Flynn², Conghui Xie³, James Lee⁶, Freya Squires⁶, Simone
Kotthaus⁷, Sue Grimmond⁷, Xinlei Ge⁴, Yele Sun³, Pingqing Fu³

10 ¹ Department of Atmospheric Sciences, School of Earth Sciences, Zhejiang University, Hangzhou,
Zhejiang, China

² Centre for Atmospheric Sciences, School of Earth and Environmental Sciences, University of
Manchester, Manchester, UK

³ Institute of Atmospheric Physics, Chinese Academy of Sciences, Beijing, China

15 ⁴ School of Environmental Science and Engineering, Nanjing University of Information Science and
Technology, Nanjing, China

⁵ National Centre for Atmospheric Science, University of Manchester, Manchester, UK

⁶ Department of Chemistry & National Centre for Atmospheric Science, University of York, York, UK

⁷ Department of Meteorology, University of Reading, UK

20

Corresponding to: Dantong Liu (dantongliu@zju.edu.cn)



Abstract

25 Black carbon (BC) is known to have major impacts on both human health and climate. The populated megacity represents the most complex anthropogenic BC emissions where the sources and related impacts are very uncertain. This study provides source attribution and characterization of BC in the Beijing urban environment during the joint UK-China APHH (Air Pollution and Human Health) project, in both winter (Nov. - Dec. 2016) and summer (May - Jun. 2017). The size-resolved mixing state of BC-containing particles was characterized by a single particle soot photometer (SP2) and their mass spectra was measured by a soot particle mass spectrometer (SP-AMS). The refractory BC (rBC) mass loading was around a factor of 2 higher in winter relative to summer and more variable coatings were present, likely as a result of additional surface emissions from the residential sector and favourable condensation in cold season. The characteristics of the BC were relatively independent of air mass direction in summer; whereas in winter the air mass from the Northern Plateau had a significant dilution effect resulting in less-coated and smaller BC, whereas the BC from the Southern Plateau had the largest core size and coatings.

We combine two online source apportionment methods for the first time, by the physical method from the SP2, and the chemical approach using the positive matrix factorization (PMF) of mass spectra from the SP-AMS. A method is proposed to isolate the BC from the transportation sector using a mode of small BC particles (core diameter $D_c < 0.18 \mu\text{m}$ and coating thickness $ct < 50\text{nm}$). This mode of BC highly correlated with NO_x concentration in both seasons ($\sim 14 \text{ ng m}^{-3} \text{ BC ppb}^{-1} \text{ NO}_x$) and corresponded with the morning traffic rush hour, contributing about 30% and 40% of the total rBC mass (35% and 55% in number) in winter and summer respectively. The BC from coal burning or biomass burning tended to dominate with moderate coatings ($ct = 50\text{-}200\text{nm}$) contributing $\sim 20\text{-}25\%$ of rBC mass. Large uncoated BC particles ($D_c > 0.18 \mu\text{m}$ and $ct < 50\text{nm}$) was more likely to be contributed by coal combustion, as these particles were not present in urban London. This mode was present in Beijing in both winter ($\sim 30\text{-}40\%$ rBC mass) and summer ($\sim 40\%$ rBC mass) but may be dominated by residential and industrial sector respectively. The contribution of BC thickly-coated with secondary species ($ct > 200\text{nm}$) to the total rBC mass increased with pollution level in winter, but was minor in summer. These large BC importantly enhanced the absorption efficiency at high pollution levels - in winter when $\text{PM}_{10} > 100 \mu\text{g m}^{-3}$ or $\text{BC} > 2 \mu\text{g m}^{-3}$, the absorption efficiency of BC increased by 25-70%. Reduction of emissions of these large BC particles and the precursors of the associated secondary coating will be an effective way of mitigating the heating effect of BC in urban environments.



1 Introduction

Black carbon aerosol (BC) has a significant impact on both climate (Bond et al., 2013) and human health (Baumgartner et al., 2014). Its regional impact in the atmosphere may be very large, especially close to polluted hotspots such as in South and East Asia, where anthropogenic emissions are high and population exposure is severe (Ramanathan and Carmichael, 2008). It has been estimated that BC over China could contribute up to 14% of the global radiative forcing budget (Li et al., 2016). Reducing BC has been postulated as a win-win policy intervention because of the shorter atmospheric lifetime of BC compared to the greenhouse gases, delivering immediate mitigation, while at the same time improving air quality (Kopp and Mauzerall, 2010).

Beijing, as one of the most populated megacities in the world has experienced severe air pollution (Yang et al., 2005; Xu et al., 1994). The complexity of emissions from multiple sectors that are often co-located (Li et al., 2017) make it extremely challenging to attribute source contributions to the BC load, hindering policy making on emission regulations. The source apportionment of BC in urban environments has been studied using both online and offline measurements and using site receptor models (Cao et al., 2005; Viana et al., 2008 and refs therein). Most of the techniques separate the fossil fuel BC, such as that from traffic sources from the solid fuel burning fraction (such as that from wood burning (Sandradewi et al., 2008; Healy et al., 2012) or open biomass burning (Schwarz et al., 2008). These techniques include using biomass burning tracers in aerosol (Puxbaum et al., 2007), or using individual organic tracer compounds to attribute the sources and provide time series representing the different sources. These are then used to segregate the different BC emission contributions by multi-linear regression (Liu et al., 2011; Laborde et al., 2013). An approach using Aethalometer measurements has been widely used based on the spectral dependence of absorption (Sandradewi et al., 2008). This technique needs to assume a prescribed absorption spectrum from traffic or wood burning sources which may be subject to variation under different burning conditions (Zotter et al., 2017). Isotope analysis of elemental carbon, in conjunction with thermal separation, allows identification of modern carbon (e.g. from biomass) from fossil fuel (from diesel or coal) based on the ^{14}C abundance (Bernardoni et al., 2013; Zhang et al., 2012). This method has been considered to be relatively unambiguous in isolating wood burning sources from traffic source, and has been used to validate the other methods in attributing elemental carbon (Liu et al., 2013; Zotter et al., 2017).

These techniques, mostly use distinct features in the chemistry or physical properties to isolate one BC source from the other, and to do so requires that there are unique characteristics that are separable. The BC sources in Beijing are combinations of residential, industrial and transport sectors (Li et al., 2017), and the fuel use could be rather more complex than two distinct sources which most techniques are based on. For example, both coal burning and diesel fuel could emit fossil fuel BC, which may not be isolated through isotope analysis, and also the absorption spectrum of BC from different sources may vary considerably and to assume a single pattern based on Aethalometer measurements may not be suitable to attribute multiple sources. The fast secondary processing of aerosols in Beijing (Sun et al., 2016b) may make the source attribution of primary BC even more challenging as the secondary coating formed on BC may alter its original source-dependent features. Given these difficulties it is unlikely that any single



methodology will give unambiguous results, but a combination of different methods may improve the understanding on the source attribution because source-specific physio-chemical properties of BC may be reflected in different ways by different methods.

It is also necessary to gain knowledge on the microphysical structure and mixing state of the soot, namely its size and what other materials are present on the individual particles, as these dictate its impact on the wider atmosphere. Other material present on a BC particle (a ‘coating’) may alter its optical properties (Liu et al., 2017), affecting the direct radiative effect on the local atmosphere, and it may also make it more susceptible to in-cloud scavenging, meaning that it can perturb the cloud properties or experience a shortened atmospheric lifetime through wet deposition (Hodnebrog et al., 2014). The source profile of size-resolved mixing state of BC is desired for the evaluation of BC properties in process models (Riemer et al., 2009) especially for environments with combined sources (Fierce et al., 2016).

This study quantifies the source attribution of BC-containing particles in urban Beijing and delivers source-specific information on their properties by combining two novel techniques, both of which directly characterize BC-containing particles but are based on physical and chemical techniques respectively. The physical technique uses a single particle soot photometer (DMT, SP2), which was previously used for source apportionment of BC in urban London (Liu et al., 2014b). This approach is to examine mixing state of BC particles as a function of their core size and this has been used to attribute the BC from traffic diesel and wood burning source. The chemical approach uses the soot particle aerosol mass spectrometer (Aerodyne, SP-AMS) which has been previously used to identify the chemical compositions of coatings associated with BC (Onasch et al., 2012a), which may be used to determine primary sources or secondary processing of BC. The combination of both techniques in this study will give the detailed physio-chemical properties of BC influenced by mixed sources. In particular, by combining the approaches the contribution of different emission sources to the optical properties of BC can be quantified and so an attribution of different sources to the BC heating in the atmospheric column can be made.

2 The site, meteorology and air mass classification

The experiments were conducted at the tower site of Institute of Atmospheric Physics (IAP), Chinese Academy of Sciences (39°58′28″N, 116°22′16″E) in Beijing during both winter (Nov.-Dec. 2016) and summer (May-Jun. 2017) periods, as part of the Air Pollution and Human Health-Beijing campaign. This site represents the typical urban Beijing environment with pollution influences from surrounding traffic, commercial activities, residential activities such as cooking and home heating and regional transport (Sun et al., 2016a).

Fig. 1a shows the terrain of the North China Plain (NCP) region to the north of Beijing and Fig. 1b shows the surface emission inventory of BC for the year 2010 (Li et al., 2017). The high anthropogenic BC emission can be generally divided by the border along Taihang and Yanshan Mountain Ridges, beyond which the region from northwest Beijing has relatively lower emissions. Considerably higher emissions are also present across the southern Plateau region. In



order to investigate the regional influence of pollutants in Beijing, the regions over the NCP and the Plateau are classified according to the terrain and BC surface emission, shown in Fig. 1c. The regions are firstly classified as the plateau and plain according to the terrain height below and above 800m, then for the region <800m, 116.5°E (the
125 longitude of central Beijing) is used to separate the Eastern and Western NCP (E and W are used as the abbreviations during the following discussion); the region >800m is separated as Northern and Southern Plateau (N and S are used as abbreviations for the following discussion) using the border along 41.5°N; the Ocean is defined as the terrain height below zero. The Northern Plateau has significantly lower emission, meaning north-westerly air mass will bring clean air into Beijing and are likely to reduce pollution levels in the city, whereas westerlies may bring
130 pollutants from the Western Plateau and south-westerlies could transport the high emissions from central China to the NCP. The local area is defined in this work as the area within the square $\pm 0.25^\circ$ away from the measurement site. BC emission inventories from different sectors are shown in Fig. S1. In winter the residential sector, which is mainly composed of residential coal burning, contributes the vast majority of BC emissions; whereas the emissions from the industrial (which also contains significant coal consumption) and transportation sectors are maintained throughout
135 the year. This means the differences in BC emissions between winter and summer will mainly result from changes in the residential sector.

The HYSPLIT backtrajectory model (Draxler and Hess, 1998) was run using the $1^\circ \times 1^\circ$ horizontal and vertical wind fields provided by the GDAS1 reanalysis meteorology. Given the emissions are intensive around the immediate Beijing area, air mass back trajectories were only followed for the previous 24-hours to examine the influence from
140 the most recent air masses. The back trajectories are then mapped onto the classified regions (Fig. 1c) to investigate variations in the potential regional source influence. The back trajectories have a 1h time resolution and each point along a single 24 hour trajectory is assigned to one of the four regional classifications. All the points along a single trajectory are then used to determine the fraction of time during the previous day that the air mass spent above each of the classified regions as shown in the bottom panel of Fig. 3a and Fig. 3b. This method has been applied previously
145 in the western Africa region to identify the potential source contributions (Liu et al., 2018). Note that the HYSPLIT analysis is not able to reproduce the dispersion of the air mass, but such effects are likely to be minimal since the trajectories are only investigated over the previous 24 hours.

Each back trajectory is assigned to be predominately from one of the regions based on a ranked classification scheme that takes account of the likely greater influence on the pollution at the receptor from closer regions with large
150 emissions. The methodology considers each region in turn, beginning with the western NCP air mass because it represents the mostly polluted region and a relatively lower air mass fraction of western NCP will make an important contribution to the pollutants measured at the receptor. If the back trajectory spent more than 10% of the previous 24 hours over the western NCP it was classified as being from that sector. The following regions are then considered in a similar way in turn based on the following order: eastern NCP, southern Plateau and northern Plateau with each
155 above 10% air mass fraction. Lastly if the air mass spent more than 20% in the local area it is defined as having significant local influence. The fraction of 10% was chosen because by varying this threshold air mass fraction $\pm 10\%$, we found this is the optimum metric to reflect the air mass influence from the classified regions.



The meteorological parameters such as wind, relative humidity (RH) and temperature were measured at ground level (z=10m) and also on the tower at z=120m. The temperature and RH at z=10m is used, but the wind at 120m is used to avoid the surface friction effect. In addition, the mixing layer height (MLH) spanning the experimental period was determined using Lidar and Ceilometer measurements (Kotthaus and Grimmond, 2018).

3 Instrumentation and data analysis

3.1 The physical properties of BC

The physical properties of individual refractory BC particles were characterized using a single particle soot photometer (SP2) manufactured by DMT Inc (Boulder, CO, USA). The instrument operation and data interpretation procedures are described elsewhere (Liu et al., 2010; McMeeking et al., 2010). The SP2 incandescence signal was calibrated for rBC mass using Aquadag® black carbon particle standards (Aqueous Deflocculated Acheson Graphite, manufactured by Acheson Inc., USA) and corrected for ambient rBC with a factor of 0.75 (Laborde et al., 2012). The mass-equivalent diameter of the rBC core (D_c) is obtained from the measured rBC mass assuming a density of 1.8 g m^{-3} (Bond and Bergstrom, 2006). For a given time window, the mass median diameter (MMD) of rBC core is calculated from the D_c distribution below and above which the rBC mass was equal.

The scattering signal of each BC particle measured by the SP2 is determined using a leading edge only (LEO) technique to reconstruct the distorted scattering signal when the particle passes through the SP2 laser beam (Gao et al., 2007). This was used to determine the scattering enhancement (E_{sca}) for each single particle which is defined as the ratio between the measured scattering of the BC particle, including any coating, and the calculated scattering resulting from the uncoated BC core (Liu et al., 2014a; Taylor et al., 2015), expressed as:

$$E_{sca} = \frac{S_{measured, coated BC}}{S_{calculated, uncoated BC}} \quad (1),$$

where the numerator is the scattering of coated BC directly measured by the SP2 and the denominator is the calculated scattering of uncoated BC core using a refractive index of BC $2.26+1.26i$ at the SP2 laser wavelength, $\lambda=1064\text{nm}$ (Moteki et al., 2010). For a given D_c , a higher E_{sca} means a thicker coating and $E_{sca}=1$ means there is no coating. The coated BC particle size (D_p) is then determined by matching the modelled scattering with the measured scattering by applying a Mie core-shell lookup table (Taylor et al., 2015).

The bulk relative coating thickness (D_p/D_c) in a given time window is calculated as the total volume of coated BC particles divided by the total volume of the rBC cores (Liu et al., 2014a), expressed as:

$$\frac{D_p}{D_c} = \sqrt[3]{\frac{\sum_i D_{p,i}^3}{\sum_i D_{c,i}^3}} \quad (2),$$



where $D_{p,i}$ and $D_{c,i}$ are the coated and rBC diameters for each single particle respectively. Note that the bulk D_p/D_c is largely independent of the uncertainties arising from smaller particles because of their less important contribution to the integrated volume.

- 190 The volume-weighted coated BC size ($D_{p,v}$) is then calculated as the product of the bulk relative coating thickness and the MMD of the BC cores, to indicate the mean coated BC size (Equation 3). The bulk mixing ratio of coating mass over rBC mass ($M_{R,bulk}$) can be also derived from D_p/D_c assuming a density of coating and rBC (Equation 4):

$$D_{p,v} = \frac{D_p}{D_c} \times MMD \quad (3),$$

$$M_{R,bulk} = \left(\left(\frac{D_p}{D_c} \right)^3 - 1 \right) \times \frac{\rho_{coating}}{\rho_{rBC}} \quad (4),$$

- 195 The mass absorption cross section at $\lambda=550\text{nm}$ (MAC^{550}) is calculated for each single particle by assuming the refractive index of rBC core $1.95+0.79i$ (Bond and Bergstrom, 2006) and coating refractive index $1.50+0i$ (Liu et al., 2015), using the Mie core-shell approach (Bohren and Huffman, 2008). Note that the absorption enhancement due to coating is considered to only occur when the coating mass over rBC mass is larger than 3 according to the recent study of (Liu et al., 2017). Fig. S3 gives the calculated MAC^{550} mapped on the $E_{sca}-D_c$ plot. The MAC^{550} in bulk for
 200 a given time window is calculated as the integrated absorption coefficient ($MAC \times m_{rBC}$) for all particles divided by the integrated particle masses, expressed by Equation (5),

$$MAC = \frac{\sum_i MAC_i \times m_{rBC,i}}{\sum_i m_{rBC,i}} \quad (5),$$

where MAC_i and $m_{rBC,i}$ are the MAC and rBC mass for each single particle respectively. This calculation is performed for each type of BC.

- 205 A PAX (Droplet Measurement Technologies, Boulder, CO, USA) (Wang et al., 2014; Selimovic et al., 2018) was deployed to directly measure the in-situ aerosol light absorption every minute using photoacoustic technology. The light-absorbing particles are heated by a laser in the acoustic chamber, and this heating produces pressure waves which are detected by a microphone. The absorption coefficient at $\lambda=870\text{nm}$ ($\sigma_{abs,870}$) is measured by the PAX. The mass absorption cross section (MAC) is determined as the absorption coefficient per unit rBC mass. Note that in this
 210 study $\sigma_{abs,870}$ values for rBC mass loadings $<0.5 \mu\text{g m}^{-3}$ were not used for MAC calculations due to the large uncertainty of absorption measurement at low concentration.

3.2 BC chemical composition

- The chemical composition of black carbon containing particles, including the refractory BC and coating compositions,
 215 are measured by a soot particle mass spectrometer (SP-AMS) (Onasch et al., 2012a; Wang et al., 2017). The results



from SP-AMS measurement during APHH are detailed in Wang et al., 2018. The SP-AMS was run in laser-only mode and so only detected compositions for BC-containing particles. In this mode the non-refractory components were not detected if they are not contained within a BC particle. The ionization efficiency (IE) and relative ionization efficiency (RIE) of sulphate and nitrate were calibrated by using ammonium nitrate and ammonium sulphate (Jayne et al., 2000). RIE of rBC was calibrated by using Regal Black (RB, REGAL 400R pigment black, Cabot Corp.) (Onasch et al., 2012b). Positive matrix factorization (PMF) (Paatero and Tapper, 1994) was applied to the mass spectra of the organic and rBC components to attribute the source contribution of BC-containing particle mass in real time, as detailed in Wang et al., 2018. Four types of BC-containing particle associated with different organic coatings were identified: fossil fuel combustion OA (FOA), biomass burning OA (BBOA), less-volatile organics (OOA1) and semi-volatile organics (OOA2) were identified. In addition, a PAH factor was also derived from the SP-AMS measurement, which is associated with coal combustion (Sun et al., 2016a).

4 Results

4.1 Overview of BC physical properties

Fig. 3 shows the temporal variation of the physical properties of BC, associated gaseous pollutants and meteorological parameters and their association with the air mass classifications. As the bottom panels show, the site was mostly influenced by northerly air masses in winter, and very few air masses came from the eastern NCP. The first half of the winter campaign up to 20th Nov. was periodically influenced by air masses from western NCP, and during the second half the synoptic meteorology shifted appreciably and was dominated by northerly (from the northern Plateau) or westerly (from the southern Plateau) air masses, with the period between 02/12 and 04/12 dominated by air from the southern Plateau. The temperature dropped from ~10°C to below 5°C when the air mass type shifted to deliver air from the plateau. In summer, Beijing received air from the western NCP, the eastern NCP and the northern plateau with southerly air masses more dominant than those from the north.

The classified air mass types are generally consistent with the local wind directions measured at 120m for both seasons (Fig. 4). In winter, the northern Plateau air masses were characterised by high speed, dry NW winds, in summer the flow was not as strong. Air masses from the southern plateau were associated with both northerly and southerly winds but with much lower wind speed and systematically higher RH than the northern plateau air masses. The south-westerly air masses also had the highest RH, which is consistent with previous observations that show air masses from lower latitudes contained more moisture in wintertime (Tao et al., 2012). In summer, air masses from the western NCP showed lower RH which may result from the almost latitudinally homogenous distribution of higher temperatures. The site showed lower wind speed and wider variation of RH when influenced by local air masses.

BC properties associated with different air mass types in both the winter and summer seasons are compared in Fig. 5. rBC mass loadings were higher in winter than in summer by around a factor of 2 for both local and regionally



transported air masses due to higher surface emissions from both the local Beijing region and the surrounding area
250 in the cold season. However, air masses from the northern Plateau during periods of strong and dry wind had notable
effect on the rBC mass in winter, greatly reducing the rBC mass in Beijing. This air mass type contributed to over
90% of the cleaner days (rBC mass concentration $< 1 \mu\text{g m}^{-3}$) in winter. This is consistent with the emission inventory
that the northwest Beijing is dominated by lower surface emissions over Mongolia. The dilution of Beijing pollution
by high wind speeds during NW air flow has been widely observed (Sun et al., 2015; Zhang et al., 2013; Zhang et al.,
255 2015). The BC particles during these periods had systematically lower core sizes (Fig. 5b1) and lower coatings (Fig.
5c1) and therefore smaller total particle sizes. This may be also as a result of more favourable removal processes for
the more coated and larger BC particles in winter.

No significant differences in the physical properties of BC particles were observed between the different air mass
types in summer, e.g. there is a consistent peak of $D_p/D_c \sim 1.4$ for all air mass types, which may suggest an almost
260 homogenous mixture or consistent BC sources across a large region around Beijing in China. In winter, the range of
 D_p/D_c values extended from similar values to those in the summer up to 2.5. The MMD of BC cores was most often
observed to be $\sim 180\text{nm}$ for both seasons, but it is noted that the air mass from the southern Plateau (as the green lines
show) had systematically larger MMD, and BC particles in air masses from this region also had the highest coatings
and largest coated BC size compared to other air masses. The observed large BC core size and coatings may be due
265 to the longer westerly transport pathways from sources in these air masses. However, the BC core size was
significantly higher in winter than in summer during periods when Beijing received air from the southern plateau.
This may result from a large contribution of residential heating activities in southern Plateau in winter which were
not present in summer

As Fig. 6 shows, the diurnal variation of rBC mass loading in winter showed a strong anti-correlation with the mixing
270 layer height (MLH), which means the BC emissions in winter were strongly diluted or concentrated by the
development or shrinking of PBL in the daytime and nighttime respectively, but the enhancement in nighttime may
also result from the increased emission from heating activities. In summer, the night-time peak of rBC mass loading
was absent but peaked during the morning rush hour which may reflect the important contribution from traffic. There
were no obvious diurnal variations in either the BC core size or coatings, suggesting BC from different sources was
275 well mixed during both seasons. In general, larger variations in the physical properties of BC were observed in winter
compared to summer.

4.2 The size distribution and mixing state of BC

Fig. 7a gives examples of BC core size distributions for typical periods in both seasons. The BC core size distribution
280 could be modelled as a single lognormal distribution:

$$\frac{dM}{d \log D_c} = A e^{\left(\frac{-\log^2(D_c/D_0)}{2 \log^2 \sigma_g} \right)} \quad (6),$$



where A is the peak concentration, D_c is the BC core size measured by the SP2, D_0 is the core MMD, σ_g is the geometric standard deviation (GSD) for the lognormal distribution. The red lines in Fig. 7a show the lognormal fit to the observations. It is noted that some fraction of the distribution at the larger end is not fitted within the single lognormal distribution, which may require an additional moment of lognormal distribution to be accounted for, as has been shown during previous urban studies (Huang et al., 2011). However, the second lognormal fitting will be subject to large uncertainty due to the saturation of the SP2 detector which has an upper cut off at $D_c=550\text{nm}$. The additional rBC mass distribution above 550nm may exist but would require instrument reconfiguration to be fully detected. The two-moment lognormal fitting is thus not performed in this study. The extrapolated rBC mass accounted for 5-8% of the total rBC mass loading which is included for the rBC mass loading reported in this study.

Fig. 7b shows the fitting parameters of BC core size distribution at different levels of rBC mass concentration. The core size was generally increased at higher rBC mass concentration but demonstrated considerable variability ranging between 150-220nm. BC particles were observed to have systematically larger core sizes in winter than in summer at the same rBC mass concentration. In winter, the significant increase of core MMD when rBC mass concentration $>5\mu\text{g m}^{-3}$ suggests possible coagulation processes are taking place at high concentration. The width of the core size distribution σ_g in winter showed a decreasing trend at higher rBC mass concentration, consistent with the view that coagulation may occur at high rBC mass concentration reducing the width of the size distribution (Pratsinis, 1988). However, in summer σ_g showed an increasing trend with rBC mass concentration, which may result from more diverse source contributions at higher rBC mass concentration. The higher σ_g in winter than in summer at the same rBC mass concentration suggests a greater complexity of sources in winter. The core sizes observed in Beijing are significantly larger than those observed in London even when the BC source profile was dominated by wood burning (170nm), which may result from other sources of BC.

Fig. 8 shows the coating content of BC was similar between seasons with $M_{R,bulk}$ 1-2 when the rBC mass concentration $<2\mu\text{g m}^{-3}$. During summer the coating thickness only periodically increased ($M_{R,bulk} >2$); but in winter the coating significantly increased particularly when the rBC mass concentration $>3\mu\text{g m}^{-3}$, showing a highly variable $M_{R,bulk}$ ranging between 1.5-10 (bulk $D_p/D_c \sim 1.4-2.6$). Accordingly, the coated BC size $D_{p,v}$ peaked at 220-310nm when rBC mass concentration $<2\mu\text{g m}^{-3}$ in both seasons, however it reached values as high as 550nm under highly polluted conditions. The large variation of BC mixing state during winter-time when the rBC mass concentration $>3\mu\text{g m}^{-3}$, may reflect the additional primary sources such as the large contribution from residential sources during the cold season. However, secondary processing of the complex source mixtures under highly polluted conditions may also play an important role in increasing the coatings.

4.3 BC segregation by size-resolved mixing state

Fig. 9 shows the BC core size-resolved mixing state during typical periods in both seasons, and the results obtained in London are also shown as a reference (Liu et al., 2014b). The BC particles were segregated according to the



discontinuous distribution in $E_{sca}-D_c$ during different periods. The criteria used is shown by the thick dashed lines in Fig. 9a. Four modes of BC could be segregated: small BC (BC_{sm}) with BC cores smaller than 180nm and coating thicknesses <50nm (assuming a core-shell structure); moderately coated BC (BC_{mod}) - moderate coating with coating thicknesses of 50-200nm; thickly coated BC (BC_{thick}) with coating thicknesses >200nm, and large uncoated BC ($BC_{lg,uncoat}$) with BC core sizes >180nm and thicknesses <50nm. The contribution of these four modes of BC particles to the total rBC number varied during different periods. In summer, the BC_{thick} only contributed a minor fraction of the total number throughout the experiment. The small, moderately coated and $BC_{lg,uncoat}$ fractions are all present in both seasons. Compared with the results in London (Fig. 9e and f), the BC_{sm} fraction was consistent with traffic influences with small core and thin coatings, and the BC_{mod} was broadly consistent with the wood burning observed in urban London. It is noted that the $BC_{lg,uncoat}$ were not significant in urban London under the different air masses or source influences observed, with the mass fraction of BC IV <8% and number fraction <3% throughout the experimental period. This means $BC_{lg,uncoat}$ may represent a source which was uniquely present in urban Beijing, however not in the UK or surrounding area.

A further analysis on the segregated BC core and coated size distribution (Fig. S2) shows the total size distribution of BC core and coated size distribution could be generally separated as three lognormal distributions with BC I+IV, BC II and BC III, representing the thin, moderate and BC_{thick} respectively. This in turn suggests the apportioned BC modes may represent discernible primary sources or sources under secondary processing.

4.4 Comparison of BC source estimation

Fig. 10 shows the temporal evolution of rBC mass determined by the SP2 and SP-AMS categorized according to the different source contributions derived in section 4.3 and as explored in Wang et al, 2018 respectively. PMF analysis on SP-AMS detected mass spectra identified four factors for BC-containing particles (Wang et al., 2018): fossil fuel BC (FOA_BC) containing BC from vehicle sources and coal burning; BC coated with biomass burning organics (BBOA_BC); BC associated with less-volatile organic coatings (OOA1_BC); and BC associated with semi-volatile organic coatings (OOA2_BC). Note that each PMF factor includes the refractory BC (C_x) and the non-refractory coatings associated with it. In order to directly compare with the rBC mass measured by the SP2, only the mass of the C_x fragments in the PMF factors are used. Table 1 shows the correlation coefficient between the different PMF factors and the SP2 segregated BC types, with green shading highlighting the high correlation ($r^2>0.6$).

The FOA_BC was not able to be further apportioned via the PMF analysis, and so this factor contains both mobile sources such as from diesel or gasoline engines, and importantly the coal burning emissions. Coal burning could result from both the residential and industrial sectors (Finkelman and Tian, 2018), with the former sector overwhelmingly dominating in winter but the contribution from the latter maintained throughout the year (Fig. S1). The small BC particle component is shown to be solely correlated with FOA_BC ($r^2=0.68$), but FOA_BC is also correlated with moderately coated and $BC_{lg,uncoat}$. The multiple correlations of FOA_BC with BC at different core



350 sizes and coating thicknesses means the fossil fuel related BC could exhibit a range of mixing states, however the BC_{sm} particle fraction that has smaller core sizes and thinner coatings tends to be only associated with and contribute to the fossil fuel BC fraction.

BBOA_{BC} which mostly resulted from open cooking sources in Beijing (He et al., 2010), is tightly correlated with BC_{mod} and the large, uncoated BC particle fraction from the SP2. Both BC types had high correlation with FOA and
355 BBOA since the fossil fuel (excluding the part correlated with BC_{sm}) and biomass burning BC particles have similar core sizes and coating contents. The potential contribution from coal burning sources are further investigated by correlating the SP-AMS measured PAH with the SP2-segregated BC types, as the PAH is considered to be an ideal marker for coal burning (Xu et al., 2006; Sun et al., 2016a). The moderately coated and BC_{lg,uncoat} fractions are found to have the highest correlation with PAH. This means the BC from coal burning tended to contribute to both the
360 moderately coated and the BC_{lg,uncoat} fractions, but not the BC_{sm}, which in turn indicates that the BC_{sm} is mainly a result of mobile sources (such as traffic) rather than coal burning. Previous studies found that the coal emission in urban China may have a larger BC core size compared to traffic sources (Wang et al., 2016). This is also consistent with the lack of the BC_{lg,uncoat} mode in urban London where there was no coal burning present in the city (Fig. 9). Given biomass burning was also correlated with moderately coated and BC_{lg,uncoat} fractions, analyses limited to the
365 size-resolved mixing state alone may not be able to distinguish the BC particles derived from coal and biomass burning in urban Beijing. This may be because the contribution of biomass burning to BC was significantly lower than that from fossil fuel in Beijing (Zhang et al., 2017), and the open biomass burning was only sporadically significant during spring and autumn harvest time over the NCP region (Chen et al., 2017). In addition, even some of the coal burning contribution, especially for the coal from residential use may be attributed as biomass burning if
370 using levoglucosan as a marker (Yan et al., 2018), which may lead to some fraction of BBOA identified by the SP-AMS containing some fraction of coal burning. BC_{mod} is consistent with wood burning in urban London but BC_{lg,uncoat} are not present from these sources (Fig. 9e and f). It is therefore more likely that the BC_{lg,uncoat} was mainly contributed by coal combustion.

The thickly coated or BC_{mod} fraction is only well correlated with the BC coated with less-volatile organics
375 (OOA1_{BC}) or semi-volatile organics (OOA2_{BC}) respectively. This means the coating composition would mostly contain less-volatile organic species when BC was thickly coated, whereas the moderate coating BC particle fraction mainly contained semi-volatile species. The coal burning or biomass burning contributions are also significant in the BC_{mod} fraction, which means these primary sources may also emit considerable semi-volatile species internally mixed with BC.

380

4.5 Diurnal variation of different types of BC

Fig. 11 shows that the diurnal variation of the four different rBC types classified by the SP2. In winter all BC types followed the diurnal evolution of MLH, whereas in summer all BC types exhibited a morning rush hour peak. For



385 BC_{thick} in winter, the average was significantly higher than the median, indicating the sporadic occurrence of the thickly coated BC. There was no discernible difference in the diurnal patterns of the absolute mass loadings of the different BC types, which means similar emission sources and the PBL development may have controlled the diurnal pattern of different BC types to a similar extent. Nevertheless, differences could be identified by relative abundances of different BC types as discussed in the following section.

390 The diurnal variation of the number or mass fraction of BC_{sm} (Fig. 11c) peaked at 8am and 7am in the winter and summer respectively, which corresponded with the morning rush hour. This is consistent with the identified possible traffic contribution to the BC_{sm} fraction by comparison with the SP-AMS factors (section 4.4). The diurnal variation of this BC mode also had high correlation with NO_x in both seasons, with the morning rush hour occurring slightly later in winter than in summer, which further confirms the likely origin of traffic source. The correlation between the NO_x concentration and different BC types is further evaluated by a multi-linear regression function, expressed as
395 Equation (7). The fitting parameters are summarized in Table 2.

$$[NO_x] = a_0 + a_1 * [small\ BC] + a_2 * [moderately\ coated\ BC] + a_3 * [thickly\ coated\ BC] + a_4 * [uncoated\ large\ BC] \quad (7)$$

Among all BC types, a_1 shows the highest value in both seasons, which indicates the strong correlation between the BC_{sm} mass fraction and the NO_x concentration, with almost identical emission factor of 68-72 ppbv $NO_x / \mu g\ m^{-3}$ of BC_{sm} . In winter, the BC_{mod} also contributed some fraction of NO_x , whereas in summer the contribution of this BC
400 type to NO_x was almost negligible. The $BC_{lg,uncoat}$ was not correlated with NO_x emission, which in turn suggests the coal combustion may not emit significant NO_x (Xu et al., 2000). The BC_{sm} fraction contributed the most in summer (50-60% in number and 40% in mass) and the second most in winter (30-40% in number and 30% in mass). These BC particles had smaller core size and thin coatings, and thus they contributed more significantly to the number than the mass. A similar fraction of the BC was also present in urban London (Liu et al., 2014b) and Paris (Laborde et al.,
405 2013) and had also been identified to be dominated by traffic sources.

BC_{mod} showed comparable contribution in both seasons (40-50% in mass or 20-25% in number). The fraction of these particles slightly increased throughout the afternoon for both seasons, and this may partly result from daytime photochemical processing, though this BC type was also significantly associated with primary sources (section 4.4). The BC_{thick} fraction showed no apparent diurnal pattern (note that BC_{thick} mass fraction in summer was minor ~5%)
410 and only made a significant contribution at higher pollution levels (section 4.6).

$BC_{lg,uncoat}$ contributed a significant mass fraction (30-40% in winter and 40% in summer) but contributed little to the number (<10%) because of the large core sizes. The mass fraction of these BC particles had a pronounced night-time peak in winter, consistent with the view that this BC type may be contributed by coal burning (also identified by comparing with the PAH factor in section 4.4), because in the cold season there was significant residential heating activities at night which may use coal as fuel (Chen et al., 2006). This night-time peak in the mass fraction of $BC_{lg,uncoat}$
415 was missing in summer due to lack of these heating activities. Nevertheless, the $BC_{lg,uncoat}$ mass fraction remained substantial in summer, comparable with that of the BC_{sm} fraction at around 40%. This may be because the coal



consumption from the industrial sector that is maintained throughout the year (Fig. S1).

To account for the dilution effect resulting from the development of the PBL, the rBC mass loading was multiplied
420 by the MLH for every half hour throughout the day. The MLH-corrected rBC mass for each BC type is shown in
Fig. 11b and provides a way of assessing the influence of BC emissions, although there are uncertainties associated
with the MLH determination from ceilometer measurement (Kotthaus and Grimmond, 2018). All BC types showed
a peak in the MLH corrected concentration at night in winter but showed a night-time minimum in summer, which
may reflect a generally higher emission during night-time in winter but not in the summer. During the daytime
425 between the hours of 6:00 and 19:00, BC_{sm} mass corrected for the MLH was similar in both seasons, suggesting that
 BC_{sm} may have comparable emission rates between seasons, consistent with the view that these BC may be dominated
by transportation sector (section 4.4). $BC_{lg,uncoat}$ had significantly higher emission at night in winter than in summer
by a factor of 2.5, also consistent with the higher coal consumption from the residential sector in winter.

430 4.6 BC at different pollution level

Given the complexity of the sources contributing to BC in Beijing, the relative primary source contributions and its
interaction with other aerosol species may vary with the overall level of pollution and this in turn may change both
the mixing state and the optical properties of BC. Fig. 12 shows mass fractions of different BC types at different PM_{10}
level determined by the total mass of AMS+SP2. The traffic-like BC_{sm} (Fig. 12a) were a constant fraction of the total
435 mass at lower pollution levels (when $PM_{10} < 50 \mu g m^{-3}$) that was around 30% and 40% in winter and summer
respectively. The decreased mass fraction of BC_{sm} at higher pollution levels is particularly marked in winter and is
because of the increased contribution of coated BC. The $BC_{lg,uncoat}$ fraction (Fig. 12b) was similar in magnitude to the
 BC_{sm} fraction in summer across all levels of pollution, which means the coal-burning like BC was almost as important
as the traffic source. In winter, the contribution of $BC_{lg,uncoat}$ mass was slightly higher than the traffic-like BC_{sm} mass
440 fraction whereas in summer the BC_{sm} mass was more significant. At the higher pollution levels in winter, some of
the $BC_{lg,uncoat}$ may be also contributed by coagulation.

The fractional mass of BC_{thick} increases substantially at higher pollution levels (Fig. 12d), especially when
 $PM_{10} > 100 \mu g m^{-3}$ with rBC mass loading $> \sim 2 \mu g m^{-3}$ and may be up to 50% of the total rBC mass. The coatings on
these BC_{thick} were largely contributed by secondary species according to the SP-AMS analysis (section 4.4). In
445 summer, lower rBC mass loadings were observed and correspondingly the BC_{thick} mass fraction was less than 10%.
The mass contribution of moderately or BC_{thick} in summer was lower than in winter at the same pollution level, which
may be due to the higher ambient temperature in summer reducing the amount of semi-volatile material partitioning
to the particles. In both seasons, the mass fraction of BC_{mod} increased with increasing PM_{10} up to $\sim 40 \mu g m^{-3}$, and
slightly decreased at $PM_{10} \sim 50 \mu g m^{-3}$ due to an increased fraction of BC_{sm} mass. At higher PM_{10} mass loadings in
450 winter, the increased mass fraction of BC_{thick} led to a decrease of moderately coated BC. However, in summer the



BC_{mod} fraction increased when PM₁ > 50 μg m⁻³, this high pollution event has previously been shown to be dominated by secondary species (Sun et al., 2015). The higher fraction of BC_{mod} in winter than in summer at the same pollution level may result from greater primary emissions (i.e. more residential coal burning in cold season) or more condensable semi-volatile species at colder temperatures.

455 The contribution of absorption coefficient is calculated based on single particle information shown in Fig. S4. It is noted that different BC types have different absorption contribution (Fig. 12 right axis) because of their varying absorption efficiency. Fig. S5 shows that the histogram of occurrence for MAC⁵⁵⁰ of each BC type during the experimental period: the BC_{sm} and largely uncoated BC had average MAC about 7.3 m²g⁻¹ and 5.3 m²g⁻¹ respectively, and BC_{lg,uncoat} had a lower MAC because of its larger core size. The moderately and BC_{thick} had average MAC of 11.2
460 m²g⁻¹ and 12.4 m²g⁻¹ respectively.

Fig. 13 shows both modelled and measured MAC⁵⁵⁰ at different pollution levels, the results agree to within 15%. For both seasons, when PM₁ < 50 μg m⁻³, the absorption efficiency of BC only increased slightly at MAC⁵⁵⁰ ~7.8 m²g⁻¹ and 7.5 m²g⁻¹ in winter and summer respectively. The MAC⁵⁵⁰ for uncoated BC was calculated to be ~6.5 m²g⁻¹ for both seasons so the enhancement of absorption efficiency (E_{abs}) is calculated as the modelled MAC⁵⁵⁰ normalized by
465 6.5 m²g⁻¹. E_{abs} significantly increased at PM₁ > 50 μg m⁻³ up to 1.5 and 1.9 for summer and winter respectively. There was a wide variability in MAC or E_{abs} at PM₁ concentrations of between 100 and 200 μg m⁻³. The generally increase in absorbing capacity of BC at higher pollution level is consistent with the findings of a recent study (Zhang et al., 2018b). The MAC⁵⁵⁰ slightly decreased at very high PM₁, i.e. >300 μg m⁻³, and this decrease is more pronounced for measurement (the grey line shows) than Mie-based modelling. This may result from the shadowing effect that the
470 very thick coating may shield the incident photons onto the absorbing core (He et al., 2015; Zhang et al., 2018a).

5 Conclusion

In order to probe the sources and processes governing atmospheric black carbon in Beijing, measurements were performed in both winter and summer using an SP2 and the core size and coating thickness were examined using the
475 single particle data. Higher rBC mass loading with more variable coatings was found in winter than in summer. The air mass from the Southern Plateau brought BC with the largest core size and coatings in winter, indicating the appreciable regional influence, whereas in summer the characteristics of BC were relatively independent of air mass direction. In contrast to equivalent measurements in London, where two particle types were observed corresponding to traffic and wood burning, other types were observed in Beijing, probably reflecting a more complex mixture of
480 sources. rBC number and mass concentrations were quantified according to the following four particle types: small thinly-coated BC, moderately-coated BC, thickly-coated BC and large thinly-coated BC. By comparison with other measurements, in particular a factorisation of coating materials from the SP-AMS, these were assigned to different soot sources.



The small thinly-coated rBC fraction was associated with traffic emissions and made up for 30% and 40% of the rBC
485 mass in winter and summer respectively. This particle fraction was strongly associated with NO_x, though the implied
ratio of 14 ng m⁻³ ppb⁻¹ was lower than the values of 18-28 ng m⁻³ ppb⁻¹ reported for London, likely due to differences
in the emissions fleet, such as a more widely used gasoline engine in Beijing (Wang et al., 2009). The large thinly-
coated rBC could be associated with coal combustion and corresponded to around 30-40% and 40% of the rBC mass
in winter and summer respectively.

490 The moderately-coated particle fraction made up 40-50% of the rBC mass and was associated with both emissions
and atmospheric processes. As a result, the original source of these particles is currently ambiguous; it is possible
that this class has multiple contributions. The thickly-coated particle fraction was mainly present during the winter
heavy haze events when PM₁ was greater than 200 μg m⁻³ or the rBC mass loading was greater than 4 μg m⁻³. During
these events, these particles made up for around 20-45% of the rBC mass and the coatings could be associated with
495 secondary species, implying that these are rBC particles that have undergone some form of atmospheric processing.
Given the thick coatings, it would be expected that these particles would exhibit higher mass absorption and scattering
coefficients, higher hygroscopicities (thus high optical thickness in the upper boundary layer) and greater scavenging
potential (thus shorter atmospheric lifetime). These large BC importantly enhanced the absorption efficiency at high
pollution levels, and reduction of emissions of these large BC particles and the precursors of the associated secondary
500 coating will be an effective way of mitigating the heating effect of BC in urban environments.

Data availability

Processed data is available through the APHH project archive at the Centre for Environmental Data Analysis
(<http://data.ceda.ac.uk/badc/aphh/data/beijing/>). Raw data is archived at the University of Manchester and is available
505 on request.

Author contributions

D.L., J.D.A., M.J.F designed the research; J.D.A., D.L. R.J. J.W. C.Y. J.D.A. H.C. M.J.F, C.X., J.L. F.S. X.G. Y.S.
and P.F. performed experiments; D.L. performed the data analysis; J.W. and X.G. analysed the SP-AMS data; S.K.
and S.G. analysed the MLH data; J.L. and F.S. analysed the NO_x and CO data; D.L., J.W. J.D.A., and H.C. wrote the
510 paper.

Acknowledgments

This work was supported through the UK Natural Environment Research Council (grant refs. NE/N007123/1,
NE/N00695X/1, NE/N00700X/1), the National Natural Science Foundation of China (41571130024, 41571130034,
515 21777073).



References

- Baumgartner, J., Zhang, Y., Schauer, J. J., Huang, W., Wang, Y., and Ezzati, M.: Highway proximity and black carbon from cookstoves as a risk factor for higher blood pressure in rural China, *Proc. Natl. Acad. Sci. USA*, **111**, 13229-13234, 2014.
- 520 Bernardoni, V., Calzolari, G., Chiari, M., Fedi, M., Lucarelli, F., Nava, S., Piazzalunga, A., Riccobono, F., Taccetti, F., and Valli, G.: Radiocarbon analysis on organic and elemental carbon in aerosol samples and source apportionment at an urban site in Northern Italy, *J. Aerosol Sci.*, **56**, 88-99, 2013.
- Bohren, C. F., and Huffman, D. R.: Absorption and scattering of light by small particles, John Wiley & Sons, 2008.
- 525 Bond, T. C., and Bergstrom, R. W.: Light absorption by carbonaceous particles: An investigative review, *Aerosol Sci. Tech.*, **40**, 27-67, 2006.
- Bond, T. C., Doherty, S. J., Fahey, D., Forster, P., Berntsen, T., DeAngelo, B., Flanner, M., Ghan, S., Kärcher, B., and Koch, D.: Bounding the role of black carbon in the climate system: A scientific assessment, *J. Geophys. Res. - Atmos.*, **118**, 5380-5552, 2013.
- 530 Cao, J., Wu, F., Chow, J., Lee, S., Li, Y., Chen, S., An, Z., Fung, K., Watson, J., and Zhu, C.: Characterization and source apportionment of atmospheric organic and elemental carbon during fall and winter of 2003 in Xi'an, China, *Atmos. Chem. Phys.*, **5**, 3127-3137, 2005.
- Chen, J., Li, C., Ristovski, Z., Milic, A., Gu, Y., Islam, M. S., Wang, S., Hao, J., Zhang, H., and He, C.: A review of biomass burning: Emissions and impacts on air quality, health and climate in China, *Sci. Tot. Environ.*, **579**, 1000-1034, 2017.
- 535 Chen, Y., Zhi, G., Feng, Y., Fu, J., Feng, J., Sheng, G., and Simoneit, B. R.: Measurements of emission factors for primary carbonaceous particles from residential raw - coal combustion in China, *Geophys. Res. Lett.*, **33**, 2006.
- Draxler, R. R., and Hess, G.: An overview of the HYSPLIT_4 modelling system for trajectories, *Aust. Meteorol. Mag.*, **47**, 295-308, 1998.
- Fierce, L., Bond, T. C., Bauer, S. E., Mena, F., and Riemer, N.: Black carbon absorption at the global scale is affected by particle-scale diversity in composition, *Nat. Commun.*, **7**, 2016.
- 540 Finkelman, R. B., and Tian, L.: The health impacts of coal use in China, *Int. Geol. Rev.*, **60**, 579-589, 2018.
- Gao, R., Schwarz, J., Kelly, K., Fahey, D., Watts, L., Thompson, T., Spackman, J., Slowik, J., Cross, E., and Han, J.-H.: A novel method for estimating light-scattering properties of soot aerosols using a modified single-particle soot photometer, *Aerosol Sci. Tech.*, **41**, 125-135, 2007.
- 545 He, C., Liou, K. N., Takano, Y., Zhang, R., Levy Zamora, M., Yang, P., Li, Q., and Leung, L. R.: Variation of the radiative properties during black carbon aging: theoretical and experimental intercomparison, *Atmos. Chem. Phys.*, **15**, 11967-11980, [10.5194/acp-15-11967-2015](https://doi.org/10.5194/acp-15-11967-2015), 2015.
- He, L.-Y., Lin, Y., Huang, X.-F., Guo, S., Xue, L., Su, Q., Hu, M., Luan, S.-J., and Zhang, Y.-H.: Characterization of high-resolution aerosol mass spectra of primary organic aerosol emissions from Chinese cooking and biomass burning, *Atmos. Chem. Phys.*, **10**, 11535-11543, 2010.
- 550 Healy, R. M., Sciare, J., Poulain, L., Kamili, K., Merkel, M., Müller, T., Wiedensohler, A., Eckhardt, S., Stohl, A., and Sarda-Estève, R.: Sources and mixing state of size-resolved elemental carbon particles in a European megacity: Paris, *Atmos. Chem. Phys.*, **12**, 1681-1700, 2012.
- Hodnebrog, Ø., Myhre, G., and Samset, B. H.: How shorter black carbon lifetime alters its climate effect, *Nat. Commun.*, **5**, 5065, 2014.
- 555 Huang, X. F., Gao, R., Schwarz, J., He, L. Y., Fahey, D., Watts, L., McComiskey, A., Cooper, O., Sun, T. L., and Zeng, L. W.: Black carbon measurements in the Pearl River Delta region of China, *J. Geophys. Res. - Atmos.*, **116**, 2011.
- Jayne, J. T., Leard, D. C., Zhang, X., Davidovits, P., Smith, K. A., Kolb, C. E., and Worsnop, D. R.: Development of an Aerosol Mass Spectrometer for Size and Composition Analysis of Submicron Particles, *Aerosol Science and Technology*, **33**, 49 - 70, [10.1016/S0021-8502\(98\)00158-X](https://doi.org/10.1016/S0021-8502(98)00158-X), 2000.
- 560 Kopp, R. E., and Mauzerall, D. L.: Assessing the climatic benefits of black carbon mitigation, *Proc. Natl. Acad. Sci. USA*, **107**, 11703-11708, 2010.
- Kotthaus, S., and Grimmond, C. S. B.: Atmospheric Boundary Layer Characteristics from Ceilometer Measurements Part 1: A new method to track mixed layer height and classify clouds, *Q. J. Roy. Meteorol. Soc.*, [10.1002/qj.3299](https://doi.org/10.1002/qj.3299), 2018.
- 565 Laborde, M., Schnaiter, M., Linke, C., Saathoff, H., Naumann, K., Möhler, O., Berlenz, S., Wagner, U., Taylor, J., and



- Liu, D.: Single Particle Soot Photometer intercomparison at the AIDA chamber, *Atmos. Meas. Tech.*, **5**, 3077-3097, 2012.
- 570 Laborde, M., Crippa, M., Tritscher, T., Jurányi, Z., Decarlo, P., Temime-Roussel, B., Marchand, N., Eckhardt, S., Stohl, A., and Baltensperger, U.: Black carbon physical properties and mixing state in the European megacity Paris, *Atmos. Chem. Phys.*, **13**, 5831-5856, 2013.
- Li, B., Gasser, T., Ciaï, P., Piao, S., Tao, S., Balkanski, Y., Hauglustaine, D., Boisier, J.-P., Chen, Z., and Huang, M.: The contribution of China's emissions to global climate forcing, *Nature*, **531**, 357-361, 2016.
- 575 Li, M., Zhang, Q., Kurokawa, J.-i., Woo, J.-H., He, K., Lu, Z., Ohara, T., Song, Y., Streets, D. G., and Carmichael, G. R.: MIX: a mosaic Asian anthropogenic emission inventory under the international collaboration framework of the MICS-Asia and HTAP, *Atmos. Chem. Phys.*, **17**, 935, 2017.
- Liu, D., Flynn, M., Gysel, M., Targino, A., Crawford, I., Bower, K., Choularton, T., Jurányi, Z., Steinbacher, M., Hüglin, C., Curtius, J., Kampus, M., Petzold, A., Weingartner, E., Baltensperger, U., and Coe, H.: Single particle characterization of black carbon aerosols at a tropospheric alpine site in Switzerland, *Atmos. Chem. Phys.*, **10**, 7389-7407, [10.5194/acp-10-7389-2010](https://doi.org/10.5194/acp-10-7389-2010), 2010.
- 580 Liu, D., Allan, J., Corris, B., Flynn, M., Andrews, E., Ogren, J., Beswick, K., Bower, K., Burgess, R., Choularton, T., Dorsey, J., Morgan, W., Williams, P. I., and Coe, H.: Carbonaceous aerosols contributed by traffic and solid fuel burning at a polluted rural site in Northwestern England, *Atmos. Chem. Phys.*, **11**, 1603-1619, [10.5194/acp-11-1603-2011](https://doi.org/10.5194/acp-11-1603-2011), 2011.
- 585 Liu, D., Li, J., Zhang, Y., Xu, Y., Liu, X., Ding, P., Shen, C., Chen, Y., Tian, C., and Zhang, G.: The use of levoglucosan and radiocarbon for source apportionment of PM_{2.5} carbonaceous aerosols at a background site in East China, *Environ. Sci. Technol.*, **47**, 10454-10461, 2013.
- Liu, D., Allan, J., Young, D., Coe, H., Beddows, D., Fleming, Z., Flynn, M., Gallagher, M., Harrison, R., and Lee, J.: Size distribution, mixing state and source apportionment of black carbon aerosol in London during wintertime, *Atmos. Chem. Phys.*, **14**, 10061-10084, 2014a.
- 590 Liu, D., Allan, J. D., Young, D. E., Coe, H., Beddows, D., Fleming, Z. L., Flynn, M. J., Gallagher, M. W., Harrison, R. M., Lee, J., Prevot, A. S. H., Taylor, J. W., Yin, J., Williams, P. I., and Zotter, P.: Size distribution, mixing state and source apportionment of black carbon aerosol in London during wintertime, *Atmos. Chem. Phys.*, **14**, 10061-10084, [10.5194/acp-14-10061-2014](https://doi.org/10.5194/acp-14-10061-2014), 2014b.
- 595 Liu, D., Taylor, J. W., Young, D. E., Flynn, M. J., Coe, H., and Allan, J. D.: The effect of complex black carbon microphysics on the determination of the optical properties of brown carbon, *Geophys. Res. Lett.*, **42**, 613-619, 2015.
- Liu, D., Whitehead, J., Alfarra, M. R., Reyes-Villegas, E., Spracklen, Dominick V., Reddington, Carly L., Kong, S., Williams, Paul I., Ting, Y.-C., Haslett, S., Taylor, Jonathan W., Flynn, Michael J., Morgan, William T., McFiggans, G., Coe, H., and Allan, James D.: Black-carbon absorption enhancement in the atmosphere determined by particle mixing state, *Nat. Geosci.*, **10**, 184-188, [10.1038/ngeo2901](https://doi.org/10.1038/ngeo2901), 2017.
- 600 Liu, D., Taylor, J. W., Crosier, J., Marsden, N., Bower, K. N., Lloyd, G., Ryder, C. L., Brooke, J. K., Cotton, R., Marenco, F., Blyth, A., Cui, Z., Estelles, V., Gallagher, M., Coe, H., and Choularton, T. W.: Aircraft and ground measurements of dust aerosols over the west African coast in summer 2015 during ICE-D and AER-D, *Atmos. Chem. Phys.*, **18**, 3817-3838, [10.5194/acp-18-3817-2018](https://doi.org/10.5194/acp-18-3817-2018), 2018.
- 605 McMeeking, G., Hamburger, T., Liu, D., Flynn, M., Morgan, W., Northway, M., Highwood, E., Krejci, R., Allan, J., and Minikin, A.: Black carbon measurements in the boundary layer over western and northern Europe, *Atmos. Chem. Phys.*, **10**, 9393-9414, 2010.
- Moteki, N., Kondo, Y., and Nakamura, S.-i.: Method to measure refractive indices of small nonspherical particles: Application to black carbon particles, *J. Aerosol Sci.*, **41**, 513-521, 2010.
- 610 Onasch, T., Trimborn, A., Fortner, E., Jayne, J., Kok, G., Williams, L., Davidovits, P., and Worsnop, D.: Soot particle aerosol mass spectrometer: development, validation, and initial application, *Aerosol Sci. Tech.*, **46**, 804-817, 2012a.
- Onasch, T. B., Trimborn, A., Fortner, E. C., Jayne, J. T., Kok, G. L., Williams, L. R., Davidovits, P., and Worsnop, D. R.: Soot particle aerosol mass spectrometer: Development, validation, and initial application, *Aerosol Science and Technology*, **46**, 804-817, [10.1080/02786826.2012.663948](https://doi.org/10.1080/02786826.2012.663948), 2012b.
- 615 Paatero, P., and Tapper, U.: Positive matrix factorization: A non-negative factor model with optimal utilization of error estimates of data values, *Environmetrics*, **5**, 111-126, [10.1002/env.3170050203](https://doi.org/10.1002/env.3170050203), 1994.



- Pratsinis, S. E.: Simultaneous nucleation, condensation, and coagulation in aerosol reactors, *J. Colloid Interf. Sci.*, 124, 416-427, 1988.
- 620 Puxbaum, H., Caseiro, A., Sánchez - Ochoa, A., Kasper - Giebl, A., Claeys, M., Gelencsér, A., Legrand, M., Preunkert, S., and Pio, C.: Levoglucosan levels at background sites in Europe for assessing the impact of biomass combustion on the European aerosol background, *J. Geophys. Res. - Atmos.*, 112, 2007.
- Ramanathan, V., and Carmichael, G.: Global and regional climate changes due to black carbon, *Nat. Geosci.*, 1, 221-227, 2008.
- 625 Riemer, N., West, M., Zaveri, R. A., and Easter, R. C.: Simulating the evolution of soot mixing state with a particle - resolved aerosol model, *J. Geophys. Res. - Atmos.*, 114, 2009.
- Sandradewi, J., Prévôt, A. S., Szidat, S., Perron, N., Alfarra, M. R., Lanz, V. A., Weingartner, E., and Baltensperger, U.: Using aerosol light absorption measurements for the quantitative determination of wood burning and traffic emission contributions to particulate matter, *Environ. Sci. Technol.*, 42, 3316-3323, 2008.
- 630 Schwarz, J., Gao, R., Spackman, J., Watts, L., Thomson, D., Fahey, D., Ryerson, T., Peischl, J., Holloway, J., and Trainer, M.: Measurement of the mixing state, mass, and optical size of individual black carbon particles in urban and biomass burning emissions, *Geophys. Res. Lett.*, 35, 2008.
- Selimovic, V., Yokelson, R. J., Warneke, C., Roberts, J. M., Gouw, J. d., Reardon, J., and Griffith, D. W.: Aerosol optical properties and trace gas emissions by PAX and OP-FTIR for laboratory-simulated western US wildfires during FIREX, *Atmos. Chem. Phys.*, 18, 2929-2948, 2018.
- 635 Sun, Y., Wang, Z., Du, W., Zhang, Q., Wang, Q., Fu, P., Pan, X., Li, J., Jayne, J., and Worsnop, D.: Long-term real-time measurements of aerosol particle composition in Beijing, China: seasonal variations, meteorological effects, and source analysis, *Atmos. Chem. Phys.*, 15, 10149-10165, 2015.
- Sun, Y., Du, W., Fu, P., Wang, Q., Li, J., Ge, X., Zhang, Q., Zhu, C., Ren, L., and Xu, W.: Primary and secondary aerosols in Beijing in winter: sources, variations and processes, *Atmos. Chem. Phys.*, 16, 8309-8329, 2016a.
- 640 Sun, Y., Wang, Z., Wild, O., Xu, W., Chen, C., Fu, P., Du, W., Zhou, L., Zhang, Q., Han, T., Wang, Q., Pan, X., Zheng, H., Li, J., Guo, X., Liu, J., and Worsnop, D. R.: "APEC Blue": Secondary Aerosol Reductions from Emission Controls in Beijing, *Sci Rep*, 6, 20668, 10.1038/srep20668, 2016b.
- Tao, M., Chen, L., Su, L., and Tao, J.: Satellite observation of regional haze pollution over the North China Plain, *J. Geophys. Res. - Atmos.*, 117, n/a-n/a, 10.1029/2012jd017915, 2012.
- 645 Taylor, J., Allan, J., Liu, D., Flynn, M., Weber, R., Zhang, X., Lefer, B., Grossberg, N., Flynn, J., and Coe, H.: Assessment of the sensitivity of core/shell parameters derived using the single-particle soot photometer to density and refractive index, *Atmos. Meas. Tech.*, 8, 1701-1718, 2015.
- Viana, M., Kuhlbusch, T., Querol, X., Alastuey, A., Harrison, R., Hopke, P., Winiwarter, W., Vallius, M., Szidat, S., and Prevot, A.: Source apportionment of particulate matter in Europe: a review of methods and results, *J. Aerosol Sci.*, 39, 827-849, 2008.
- 650 Wang, J., Zhang, Q., Chen, M., Collier, S., Zhou, S., Ge, X., Xu, J., Shi, J., Xie, C., Hu, J., Ge, S., Sun, Y., and Coe, H.: First Chemical Characterization of Refractory Black Carbon Aerosols and Associated Coatings over the Tibetan Plateau (4730 m a.s.l), *Environ. Sci. Technol.*, 51, 14072-14082, 10.1021/acs.est.7b03973, 2017.
- 655 Wang, J., Liu, D., Ge, X., Wu, Y., Shen, F., Chen, M., Zhao, J., Xie, C., Wang, Q., Xu, W., Zhang, J., Hu, J., Allan, J., Joshi, R., Fu, P., Coe, H., and Sun, Y.: Characterization of black carbon-containing fine particles in Beijing during wintertime, *Atmos. Chem. Phys. Discuss.*, <https://doi.org/10.5194/acp-2018-800>, in review, 2018.
- Wang, Q., Huang, R. J., Cao, J., Han, Y., Wang, G., Li, G., Wang, Y., Dai, W., Zhang, R., and Zhou, Y.: Mixing State of Black Carbon Aerosol in a Heavily Polluted Urban Area of China: Implications for Light Absorption Enhancement, *Aerosol Sci. Tech.*, 48, 689-697, 10.1080/02786826.2014.917758, 2014.
- 660 Wang, Q., Huang, R. J., Zhao, Z., Cao, J., Ni, H., Tie, X., Zhao, S., Su, X., Han, Y., and Shen, Z.: Physicochemical characteristics of black carbon aerosol and its radiative impact in a polluted urban area of China, *J. Geophys. Res. - Atmos.*, 121, 2016.
- Wang, X., Westerdahl, D., Chen, L. C., Wu, Y., Hao, J., Pan, X., Guo, X., and Zhang, K. M.: Evaluating the air quality impacts of the 2008 Beijing Olympic Games: On-road emission factors and black carbon profiles, *Atmos. Environ.*, 43, 4535-4543, 2009.
- 665 Xu, S., Liu, W., and Tao, S.: Emission of polycyclic aromatic hydrocarbons in China, *Environ. Sci. Technol.*, 40, 702-708, 2006.



- Xu, X., Gao, J., Gao, J., and Chen, Y.: Air pollution and daily mortality in residential areas of Beijing, China, *Archives of Environmental Health: An International Journal*, 49, 216-222, 1994.
- 670 Xu, X., Chen, C., Qi, H., He, R., You, C., and Xiang, G.: Development of coal combustion pollution control for SO₂ and NO_x in China, *Fuel Processing Technology*, 62, 153-160, 2000.
- Yan, C., Zheng, M., Sullivan, A. P., Shen, G., Chen, Y., Wang, S., Zhao, B., Cai, S., Desyaterik, Y., and Li, X.: Residential Coal Combustion as a Source of Levoglucosan in China, *Environ. Sci. Technol.*, 52, 1665-1674, 2018.
- 675 Yang, J., McBride, J., Zhou, J., and Sun, Z.: The urban forest in Beijing and its role in air pollution reduction, *Urban forestry & urban greening*, 3, 65-78, 2005.
- Zhang, Q., Quan, J., Tie, X., Li, X., Liu, Q., Gao, Y., and Zhao, D.: Effects of meteorology and secondary particle formation on visibility during heavy haze events in Beijing, China, *Sci. Tot. Environ.*, 502, 578-584, 2015.
- Zhang, R., Jing, J., Tao, J., Hsu, S.-C., Wang, G., Cao, J., Lee, C. S. L., Zhu, L., Chen, Z., and Zhao, Y.: Chemical characterization and source apportionment of PM 2.5 in Beijing: seasonal perspective, *Atmos. Chem. Phys.*, 13, 7053-7074, 2013.
- 680 Zhang, X., Mao, M., Yin, Y., and Wang, B.: Numerical Investigation on Absorption Enhancement of Black Carbon Aerosols Partially Coated With Nonabsorbing Organics, *J. Geophys. Res. - Atmos.*, 123, 1297-1308, 10.1002/2017jd027833, 2018a.
- 685 Zhang, Y., Perron, N., Ciobanu, V., Zotter, P., Minguillón, M., Wacker, L., Prévôt, A., Baltensperger, U., and Szidat, S.: On the isolation of OC and EC and the optimal strategy of radiocarbon-based source apportionment of carbonaceous aerosols, *Atmos. Chem. Phys.*, 12, 10841-10856, 2012.
- Zhang, Y., Ren, H., Sun, Y., Cao, F., Chang, Y., Liu, S., Lee, X., Agrios, K., Kawamura, K., Liu, D., Ren, L., Du, W., Wang, Z., Prevot, A. S. H., Szidat, S., and Fu, P.: High Contribution of Nonfossil Sources to Submicrometer Organic Aerosols in Beijing, China, *Environ. Sci. Technol.*, 51, 7842-7852, 10.1021/acs.est.7b01517, 2017.
- 690 Zhang, Y., Zhang, Q., Cheng, Y., Su, H., Li, H., Li, M., Zhang, X., Ding, A., and He, K.: Amplification of light absorption of black carbon associated with air pollution, *Atmos. Chem. Phys.*, 18, 9879-9896, 10.5194/acp-18-9879-2018, 2018b.
- Zotter, P., Herich, H., Gysel, M., El-Haddad, I., Zhang, Y., Močnik, G., Hüglin, C., Baltensperger, U., Szidat, S., and Prévôt, A. S. H.: Evaluation of the absorption Ångström exponents for traffic and wood burning in the Aethalometer-based source apportionment using radiocarbon measurements of ambient aerosol, *Atmos. Chem. Phys.*, 17, 4229-4249, 10.5194/acp-17-4229-2017, 2017.
- 695



R^2 (N=1406)	FOA_BC (fossil fuel)	BBOA_BC (biomass burning)	OOA1_BC (less volatile)	OOA2_BC (semi-volatile)	PAH_BC
Small BC	0.68	0.55	0.10	0.12	0.47
Moderately coated BC	0.61	0.66	0.40	0.63	0.81
Thickly coated BC	0.31	0.54	0.61	0.47	0.59
Large uncoated BC	0.79	0.85	0.42	0.34	0.82
BCmass total	0.74	0.85	0.51	0.51	0.89

700

Table 1. (a) Pearson's correlation coefficients between the time series of SP2 and SP-AMS segregated rBC mass and PAH. The correlations with Pearson $r^2 > 0.6$ are shaded in green. All correlations are significant at the 0.01 level (2-tailed).

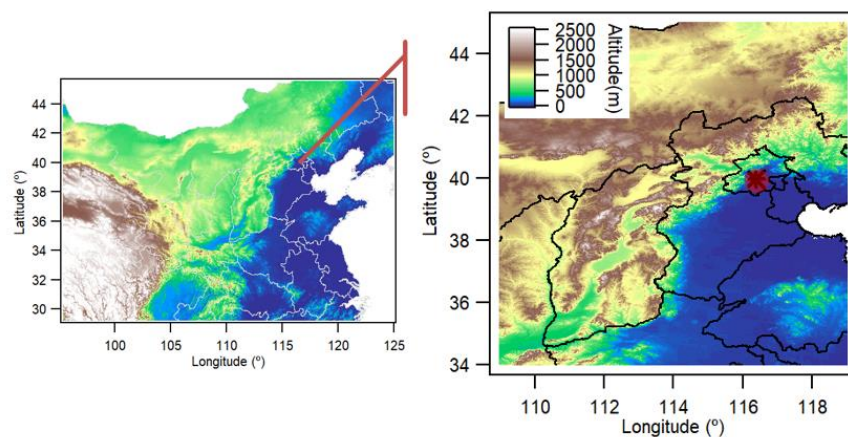
705

NO _x with BC types	a1	a2	a3	a4	a0
winter	72.3 ± 3.2	21.3 ± 3.0	16.3 ± 2.1	0	8.8 ± 1.3
summer	68.4 ± 4.7	0	0	0	1.15 ± 0.77

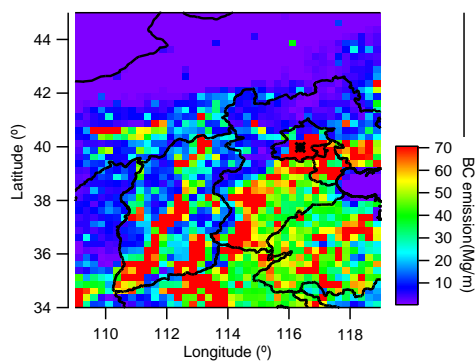
Table 2. Multi-linear regression for Equation (7) among NO_x and different BC types.



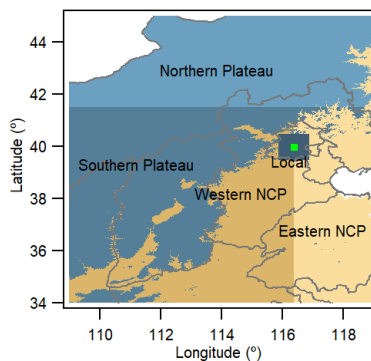
710 (a)



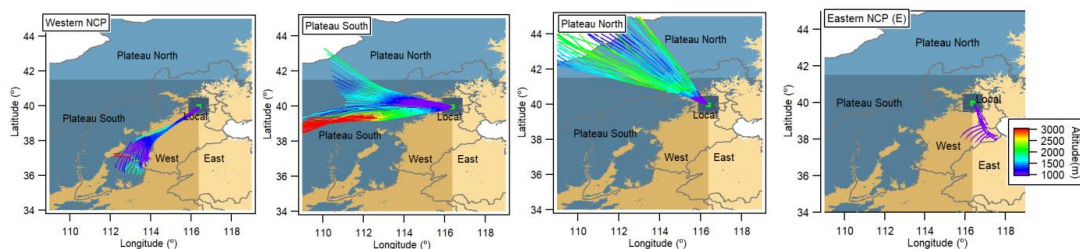
(b)



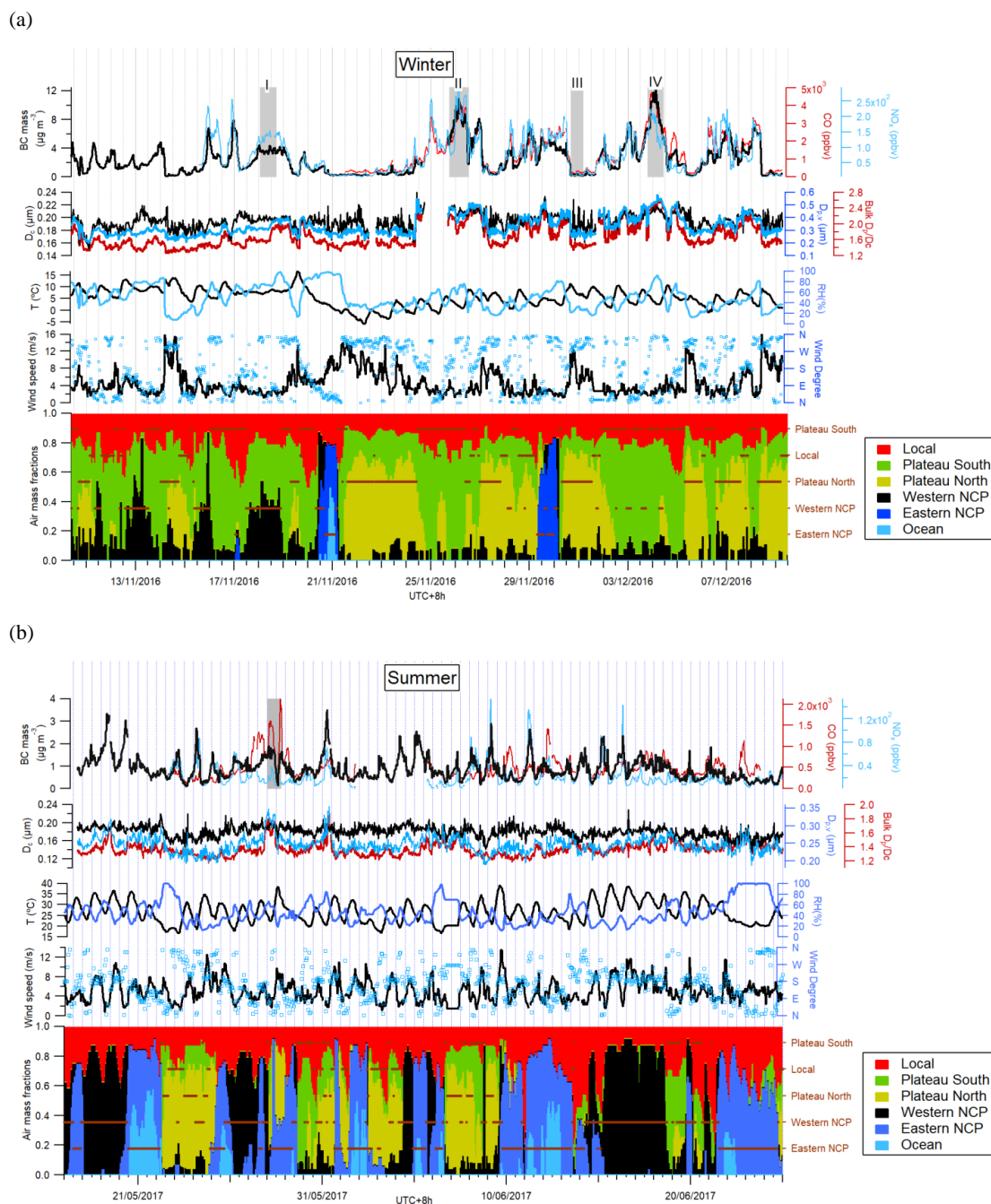
(c)



715 Figure 1. (a) Terrain height for the North China Plain (NCP) and the Plateau; (b) BC emissions from all sectors in 2010; (c) the regional classification according to terrain height and emission.



720 Figure 2. Classified air mass origins based on back trajectory analysis: western NCP, Southern Plateau, Northern Plateau and Eastern NCP.



725 Figure 3. Time series of BC-related properties in the winter (a) and summer (b) experiments. From top to bottom subpanels: BC mass loading, CO and NO_x; BC bulk D_p/D_c , core MMD and coated volume-equivalent diameter; ambient temperature and RH at $z=8$ m; wind speed and direction at $z=120$ m; air mass fractions from different origins



based on back trajectory analysis, with the brown horizontal lines indicating the classified air mass types. The vertical grey shades mark the periods for the detailed mixing state analysis in Fig. 9.

730

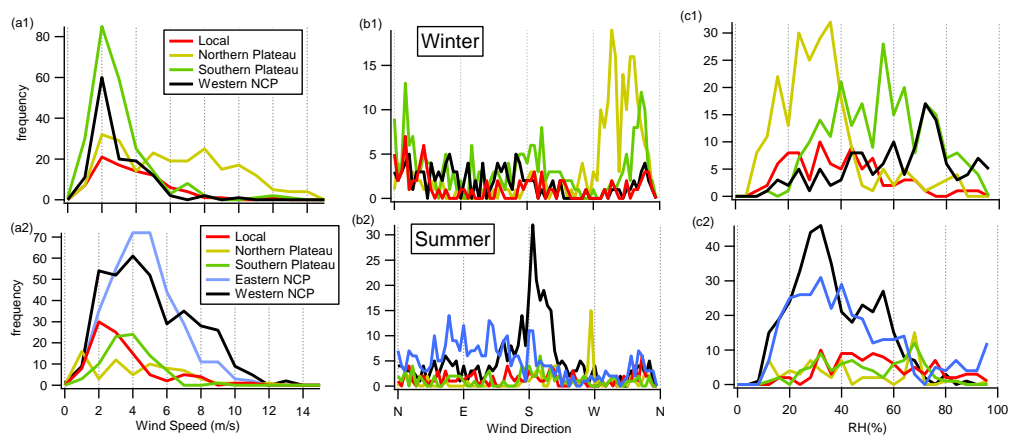
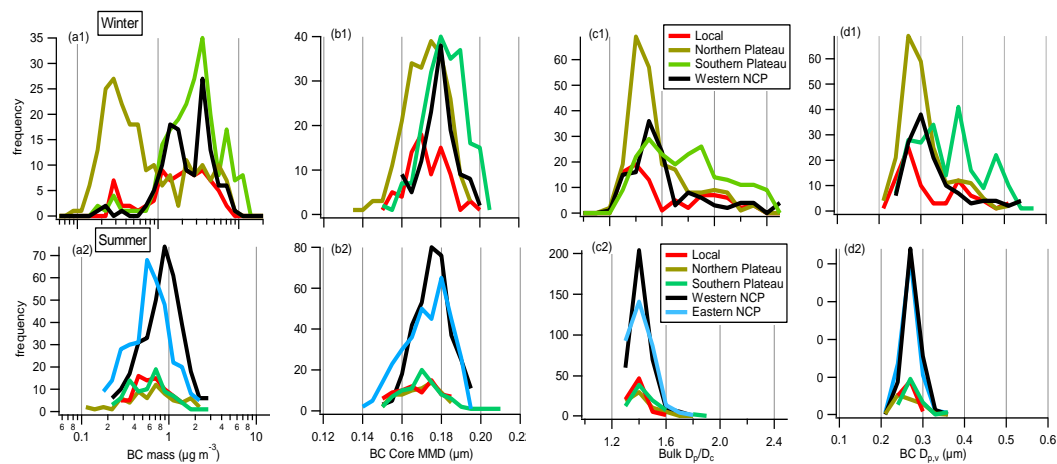
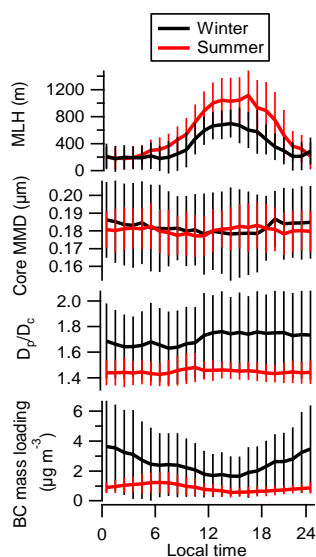


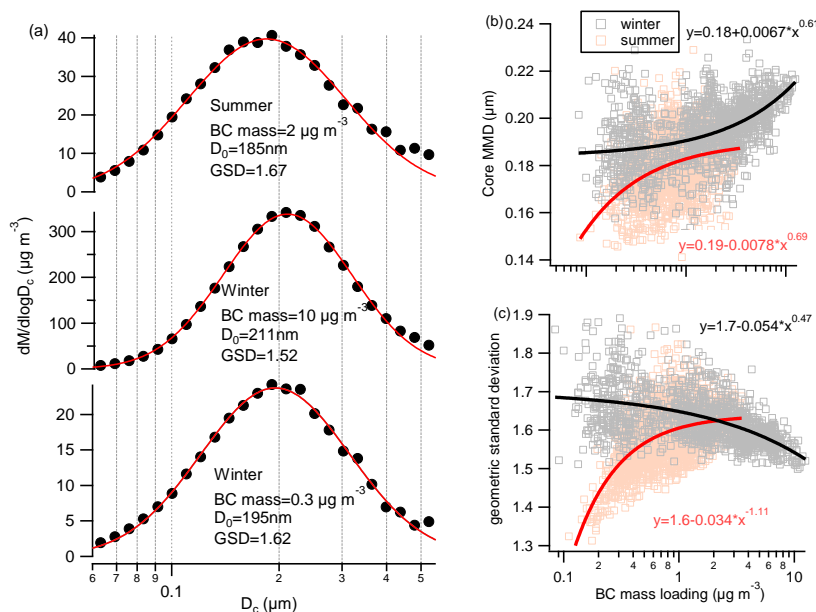
Figure 4. Frequency distributions of wind speed and direction ($z=120$ m) and RH ($z=8$ m) for classified air mass types in both seasons.



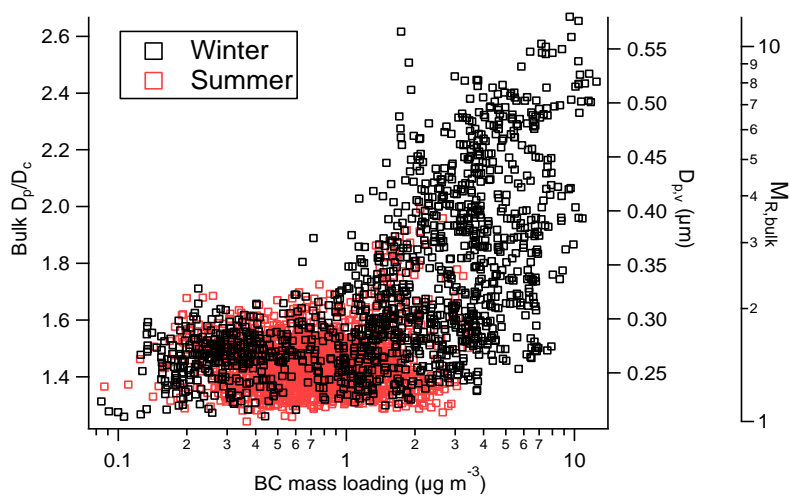
735 Figure 5. Histograms of BC mass loading, core size MMD, D_p/D_c and $D_{p,v}$ for different air masses in both seasons.



740 Figure 6. Diurnal variations of mixing layer height (MLH) and BC-related properties in winter and summer. The lines show the mean at each hour and error bars denote $\pm 1\sigma$.



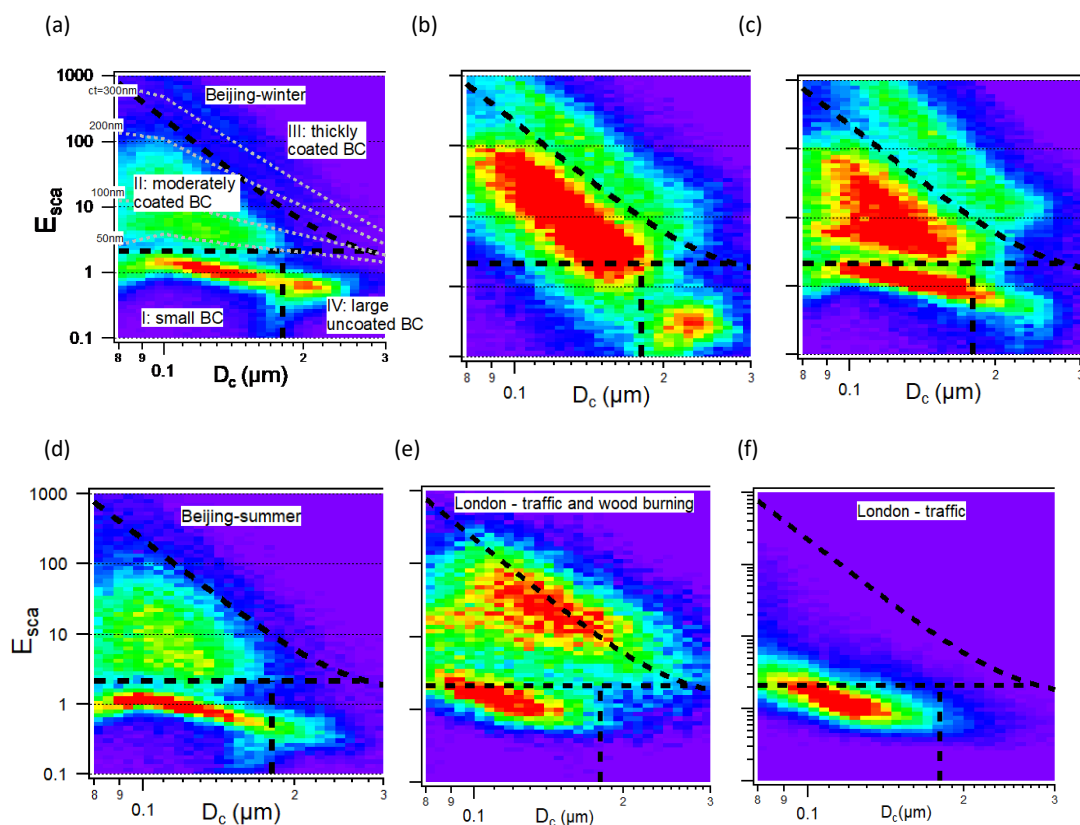
745 Figure 7. (a) BC core size distribution averaged over different rBC mass loading conditions in both seasons, showing the lognormal fitting and the fitted peak diameter (D_0) and geometric standard deviation (GSD); (b) BC core MMD as a function of BC mass loading and parameterization; (c) BC core GSD (from the fitting) as a function of BC mass loading and their fitting functions.



750 Figure 8. Mixing status of BC at different levels of BC mass loading in both seasons, with different y-axes showing bulk D_p/D_c , volume-weighted coated particle size ($D_{p,v}$) and bulk mass mixing ratio of coating/rBC.

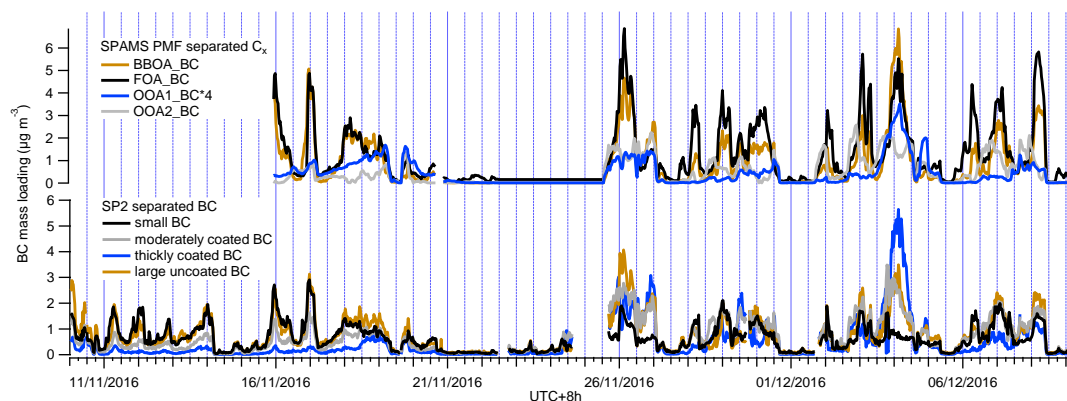


755

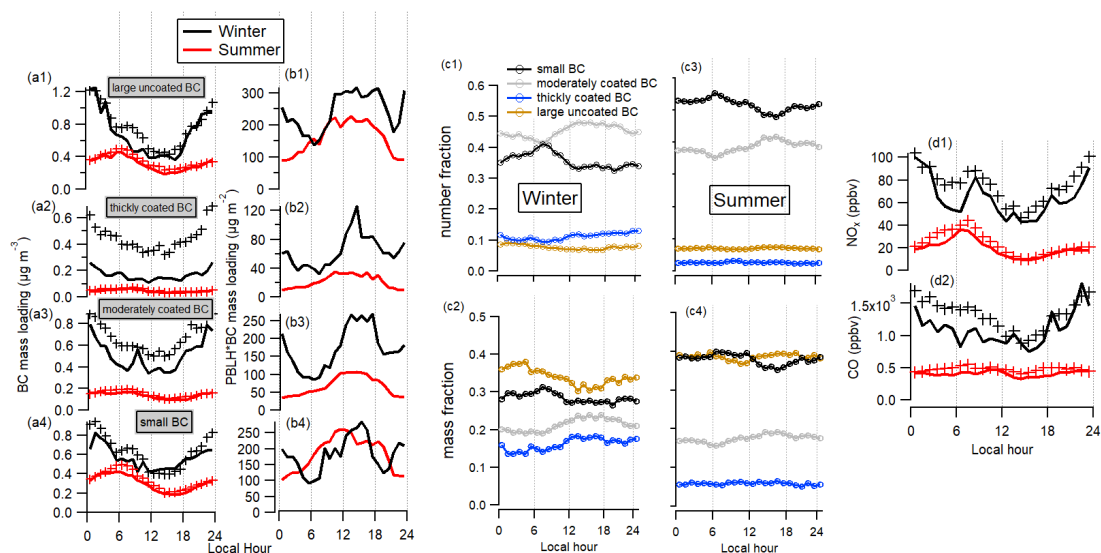


760

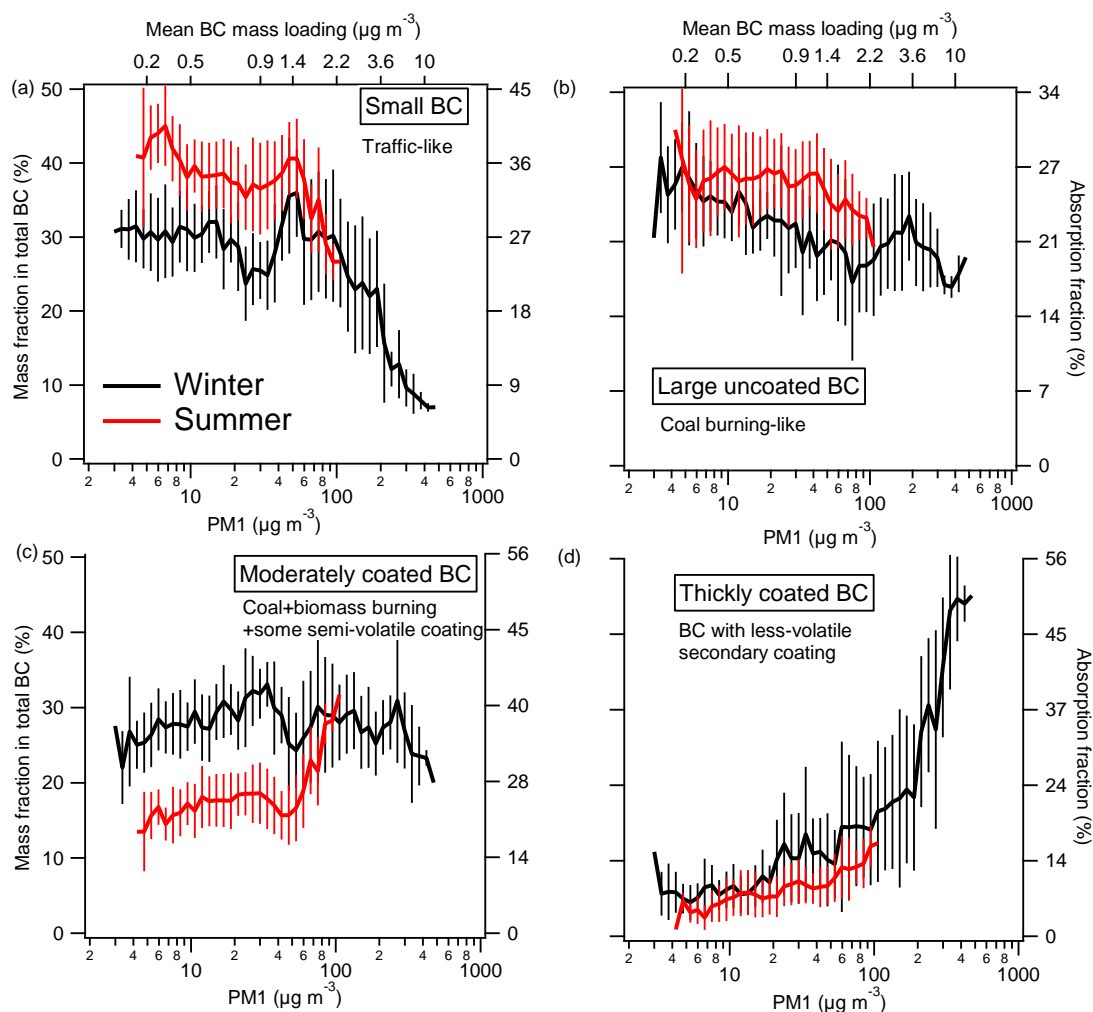
Figure 9. Scattering enhancement (E_{sca}) as a function of BC core size (D_c) for the three periods (as period I-III indicated in Fig. 3) in Beijing winter (a-c), Beijing summer (d), London with mixed sources (e) and London with traffic source (f). Each plot is coloured by particle number density. The particles are separated as four groups using the borders (from top to bottom) at $y=3.38+0.000436*x^{-5.7}$, $y=2.1$, $x=0.18$, as shown by dashed lines on each plot. The grey dashed lines on (a) denote coating thicknesses mapped on E_{sca} - D_c plot.



765 Figure 10. Time series of SP2-separated rBC mass and SP-AMS separated C_x mass by PMF analysis.



770 Figure 11. Diurnal variation of the rBC mass segregated by their SP2 characteristics in both seasons. a) shows the median (solid line) and mean (markers) at each hour; b) the median value of PBLH-corrected rBC mass; c) the number and mass fractions for each BC type; d) the NO_x and CO.



775 Fig. 12. The mass (left y-axis) and absorption (right y-axis) contributions of different BC types at different pollution levels. The mass fraction of each BC type is the average \pm standard deviation at each PM₁ bin. The top axis shows the averaged rBC mass loading at each PM₁ bin, and the right axis indicates the average absorption fraction corresponding with each rBC mass fraction.

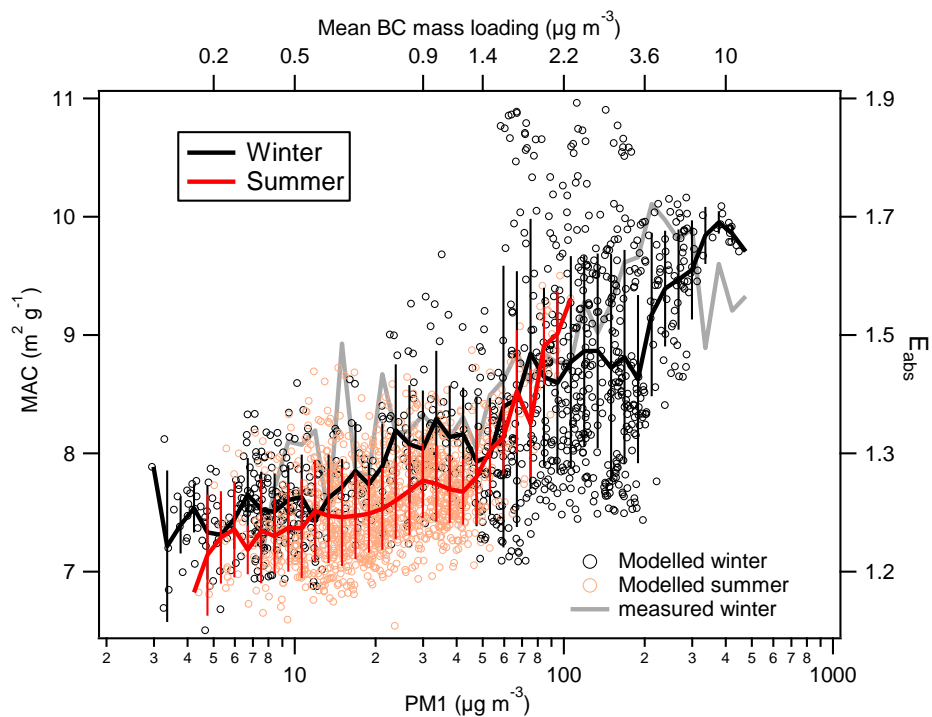


Fig. 13. The modelled and measured MAC^{550} and E_{abs} at different pollution level.